Renewable Energy 207 (2023) 471–483

Contents lists available at ScienceDirect

Renewable Energy

journal homepage: www.elsevier.com/locate/renene

Rigorous simulation of geothermal power plants to evaluate environmental performance of alternative configurations

Marco Vaccari [a,*], Gabriele Pannocchia [a,*], Leonardo Tognotti [a], Marco Paci [b]

[a] University of Pisa, Department of Civil and Industrial Engineering, Largo Lucio Lazzarino 2, 56126 Pisa, Italy
[b] Enel Green Power, Via Andrea Pisano 120, 56122 Pisa, Italy

ARTICLE INFO

Keywords:
Geothermal system
Geothermal power plant
Digital twin
Simulation
Environment
Life-cycle assessment

ABSTRACT

Different studies highlighted the environmental impacts of geothermal power plants (GPPs), especially in the operational phase. Primary data are essential for reliable environmental assessments, but these are not available when considering alternative configurations. Rigorous simulation can offer such a degree of information, representing also a tool for a digital twin technology transition. Considering a GPP in Tuscany, Italy, four alternatives configurations are simulated in UniSim Design®, performing accurate refinements to the thermodynamic model to properly estimate the behavior of different pollutants (Hg, H_2S, NH_3, and SO_2) among the various unit operations. The configurations alternate direct-contact and surface condensers as well as wet and dry towers as cooling systems, while a fifth one adopts an organic Rankine cycle. The actual plant model has been reconciliated with data collected during two different monitoring campaigns. Performance analysis shows a trade-off: the lowest pollutant emissions are obtained using the dry tower generating less net energy (20.17 MWe and 20.83 MWe), instead, adopting surface condenser and wet tower, 22.26 MWe are produced with NH_3 emissions almost 3 times the measured ones. The CO_2 and CH_4 amount in the well fluid is not abated in any configurations and therefore their emissions are the same among them.

1. Introduction

Energy production is increasingly in need to find sustainable ways to be performed and geothermal power generation represents a widely spread technology across the world [1]. Even if still small in comparison to the many countries that use their thermal resources for district or space heating, the number of nations now using geothermal energy to generate electricity is increased in the last 5 years. Clearly, no technology is free of adverse environmental impacts [2], and geothermal energy production is linked mainly to land use, gaseous emissions, and liquid discharges that can negatively affect agricultural lands [3].

Qualitative and quantitative measurements are required in every stage for defining an accurate and reliable baseline and monitoring the natural background (or fugitive) emissions [4]. As example, both local geological characteristics and methodological choices inherent to a life-cycle assessment (LCA) methodology, i.e., the definition of the functional units, the system boundaries, the life span, and the impact assessment method, highly affect the life-cycle environmental impacts studies [4]. The large variability of reported results on environmental performance across studies makes it difficult to define a holistic science-based approach to address LCA of geothermal power plants (GPPs) [5], such that specific guidelines based on experts' knowledge have been defined. A method combining exergy analysis with LCA and applied on a binary GPP in Turkey showed how the main environmental impact is represented by the non-condensable gases (NCG) released into the atmosphere during the operational phase [6]. Moreover, the outcomes of the study point out a decreased environmental effect of the system when the ambient temperature decreases and the brine inlet temperature increases. Even for geothermal systems utilization dedicated to space heating, the analysis of economy, thermal efficiency, and environmental impact have to be performed using simulations forecasting life-cycle trends [7]. The study assesses the carbon intensity of geothermal systems over their life cycles determining that the drilling process is the main carbon emission source.

A specific comparison performed on Italian GPPs against other renewable energy systems, showed how the most impacting categories for the GPP are terrestrial acidification, human toxicity, marine, and freshwater eco-toxicity [8]. Due to the difficulty of collecting inventory data, most such LCA studies are developed based on secondary data, that is, by reworking published results. Colucci et al. [9] used an inventory published in 2012 for the old configuration of a GPP in

* Corresponding authors.
E-mail addresses: marco.vaccari@ing.unipi.it (M. Vaccari), gabriele.pannocchia@unipi.it (G. Pannocchia), leonardo.tognotti@unipi.it (L. Tognotti), marco.paci@enel.com (M. Paci).

https://doi.org/10.1016/j.renene.2023.03.038
Received 12 September 2022; Received in revised form 4 March 2023; Accepted 8 March 2023
Available online 10 March 2023

Nomenclature

Acronyms

AMIS®	Mercury and Hydrogen sulfide abatement system
DCDry	Alternative configuration with Direct-Contact condenser and Dry tower
EGP	ENEL Green Power
EOS	Equation of State
GPP	Geothermal power plant
LCA	Life-cycle assessment
NCG	Non-condensable gases
ORC	Organic Rankine Cycle
ORCDry	Alternative configuration with ORC and Dry towers
PFD	Process Flow Diagram
PR	Peng–Robinson
SDry	Alternative configuration with Surface condenser and Dry tower
SWet	Alternative configuration with Surface condenser and Wet towers
BG4	GPP Bagnore 4

Symbols

F	Flow
N_S	Number of *Tower* stages
P	Pressure
T	Temperature
V	Volume

Greek Letters

η_S	*Tower* stages efficiency
η_K	*K-100* and *K-101* efficiencies, gas extractor compression stages
$\xi_{TEE,i}$	Split parameters in *TEE-100* referring to stream i
Φ	Data reconciliation objective function
ϕ_i	Value of ith variable at a given instant
$\bar{\phi}_i$	Reference value for ith variable
Δ	Percentage deviation of the considered predicted variable from its measurement

Subscripts

max	Maximum
min	Minimum
aq	Aqueous
g	Gaseous
l	Liquid
Hg, j	Related to Mercury in the stream j
e	Electrical energy
m	Mechanical energy
th	Thermal energy

Iceland to evaluate a project regarding the facility update and evaluated that introducing new technology for abatement and re-injection moderately improved the emission of CO_2 and H_2S. Clearly, the best option is to collect primary data by the means of accurate surveys and questionnaires addressed to the plant operator [10]. A study revealed that more than 95% of the potential environmental impacts of a single flash GPP are coming from the operational (direct emissions to air of NH_3, CH_4, CO_2) and development (CO_2 emissions due to diesel combustion during drilling) phases [10].

Nevertheless, these studies are performed at a level of detail that is not able to catch the different implications that alternative technologies solutions and schemes may rise in terms of impacts, especially in the operational phase. On the other hand, to the best of the authors knowledge, the literature lacks detailed simulations studies that can provide the answers to the aforementioned questions. In particular, given the significant level of variability in the analytical determination of the atmospheric emissions connected with the operational phase of the GPPs [11], a recent detailed process simulation model was developed based on real data from a GPP, aimed mainly at evaluating mercury emissions from evaporative towers [12]. As a matter of fact, simulation of GPPs has become an excellent tool to monitor and control the emission of pollutants, exploiting the different thermodynamical models implemented in commercial softwares [13]. Besides, the design of efficient energy systems nowadays cannot deny the importance of a digital twin that interactively translates the needs and preferences of decision makers into an optimization-based model generating meaningful solutions [14]. For instance, a real-time monitoring and control method using a digital twin has been proposed during the phase of geothermal drilling [15]. Thus, the importance of a detailed and rigorous simulation is explained, given an actual GPP configuration, since the operating and environmental conditions vary while different pollutants of interest, mostly NCG, must be monitored due to regulatory purposes [12]. Hence, to compare and test different, possibly less impacting, alternative solutions in terms of environmental and energetic performances, an approach to describe detailed plant equipment and interconnections can better suggest information to be used for the inventory of new projects.

For all such reasons, this paper presents and compares different detailed process simulation models of GPPs built on alternative schemes proposed by the geothermal operator Enel Green Power (EGP) for a real GPP in Tuscany, Italy. The actual configuration of the GPP is modeled using real data taken from EGP in different seasonal conditions to best perform a data reconciliation procedure.

2. The geothermal process

2.1. The geothermal cycle

The main differences among GPP process cycles consist of the nature and conditions of the well-water geothermal fluid. When the vapor phase is relevant a first phases separation is needed (the so-called "flash plant" [16]), otherwise if the liquid fraction is predominant the conversion of thermal to mechanical power takes place in a completely separate circuit (so-called "binary" cycle [17]).

Maximizing the energy production and exergy efficiency of both configurations have been deeply studied in the literature. A thermodynamic performance and techno-economic analysis of different GPP systems (double-flash, flash-ORC, and double-flash-ORC) highlighted that the double-flash systems show an obvious advantage in terms of net electric power produced and economic parameters [18]. Another recent work studied the effect of flash and evaporator outlet temperatures on the produced net power, considering the levelized cost of energy as an index [19]. A single-flash GPP in Indonesia has been studied for contemplating an upgrade to a double-flash system [20] or for setting the optimal turbine inlet pressure to minimize the effects of irreversibility and exergetic efficiency of the ambient temperature on each component [21]. A parametric study on a double-flash binary GPP outlined how the net energy production and exergy efficiency of the system with an ejector–expander integrated into the conventional expansion valve have a maximum in a specified pressure value [22].

Using the Simulated Annealing algorithm, the thermodynamic performance of a binary GPP in Turkey has been optimized by adjusting

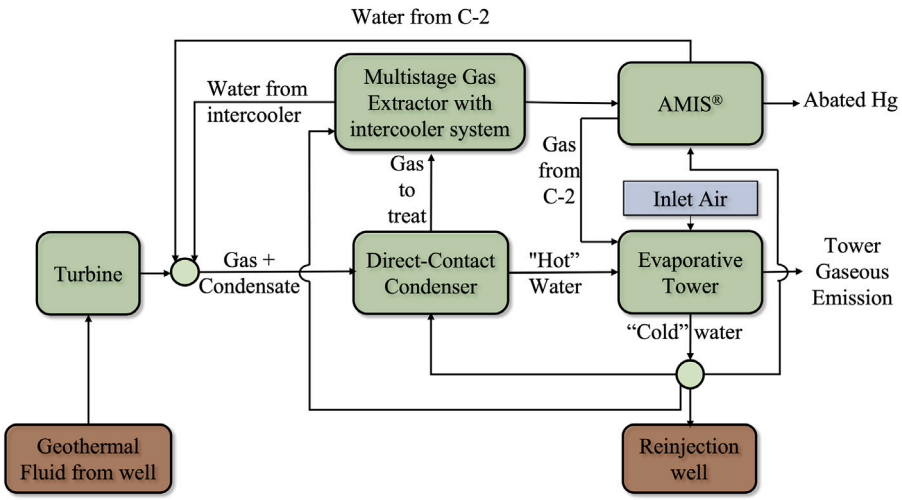

Fig. 1. PFD of the considered GPP. The dots represent mixer or splitters of the streams.

the pressure differences and the mass flow of the ORC, doubling the exergy efficiency while reducing the NCG emission rate [23]. Still in Turkey, an artificial neural network model of a GPP performed numerically on Matlab was used to find the best system operation condition that improved the net power generation by more than 20% [24]. The thermo-economic comparison between the ORC and binary flashing cycle for possible application in a GPP in China, showed a trade-off of thermodynamic and economic performance, evidencing how the yield of the two systems is maximized at different operating characteristics [25].

Dynamic simulation was used to evaluate the impact of the CO_2 content on the power consumption of the reinjection process in a GPP in Italy by performing a sensitivity analysis [26]. Modeling and simulation of GPP were also recently used to formulate new designs for a double-flash binary system and study the irreversibility of such proposed designs [27]. Also, the investigation of the economic feasibility of complete municipal energy autonomy in an energy system including GPPs in Germany was performed using a generic optimization model [28].

Pollutants emission from GPP has also been explored, whereas different system layouts are tested on an existing plant to minimize the lowest excess deposit of silica [29], or two greenfield plant layouts are investigated for the utilization of a high enthalpy liquid-dominated reservoir minimizing the NCG emission [30]. Finally, a complete review on the state-of-the-art of GPP can be found in [31].

2.2. The considered GPP and its operating conditions

The GPP considered in this paper is *Bagnore 4* (later on indicated as BG4), located in the Mt. Amiata, Tuscany, and, as many systems employed in Italy, it includes a direct steam condensation cycle with consequent release of the NCG present in the feeding geothermal fluid into the atmosphere (see Fig. 1 for a simplified process flow diagram (PFD)).

The geothermal fluid, mostly in vapor phase, fed to the GPP is first expanded in a turbine and then condensed at vacuum conditions in a direct-contact condenser. At this point, the NCG naturally present in the well fluid, are extracted via a multi-stage centrifugal compressor and conveyed to the mercury and hydrogen sulfide abatement system (AMIS®) [32]. This system consists of two main parts: the abatement of Hg in an activated carbon absorber at about 30 °C, and the oxidation of H_2S to SO_2 at 200 – 250 °C, which is subsequently removed in a washing packed tower (C-2). Two NCG present in the geothermal fluid in nonnegligible quantities are Hg, which its natural presence has been enhanced by the minero-metallurgical activity of cinnabar on Mt. Amiata, and NH_3.

The emissions into the atmosphere comes from the evaporative tower (three wet type cells for each 20 MW group), which constitutes the cooling system of the GPP: some in gaseous form (H_2, CO_2, CH_4, N_2, Ar, O_2, residual H_2S and Hg vapors) and other in aerosol form (NH_3 and As). The emission control is performed by the aforementioned AMIS®, and secondly by the application of demister at the top of the cooling tower to solve the problem of aerosol spills.

The liquid phase stream leaving the condenser is pumped directly on top of the cooling tower complex. Here, encountering the gaseous stream exiting the AMIS® and the ascending air flow of induced by fans, part of it evaporates (about 19 – 25 kg/s) and the remaining part cools down to about 30 °C. The cooled water is collected in a tank, portioned and sent: as cooling fluid in the condenser and in the intercooler stage of the gas extractor, as washing fluid in the C-2 of the AMIS®, and, finally, to re-injection into the wells. Clearly, the amount of water evaporated strongly depends on both the temperature and the humidity of the atmospheric air intake, highly affecting the performances in terms of NCG emission [12].

The gas draft of the extractor maintains the vacuum conditions in the condenser and, since its motors work at constant revolutions, ambient temperature plays a key role on the pressure value (40–120 mbar from winter to summer) [12]. Because of the phase equilibria established by direct mixing, the streams exiting the condenser do not share the same temperature, that is, the hot water is usually in the range 30–37 °C while gaseous stream is colder (27–34 °C).

3. Power plant model

To evaluate operational (energy consumption and net power produced) and environmental performances (emissions of Hg, H_2S, NH_3, and SO_2 from evaporation towers) of a GPP, a detailed process simulation model is built. This allows us to analyze the distribution of both energy consumption and pollutants among the various unit operations for the actual GPP and the various alternative plant configurations simulated.

The model is implemented using UniSim Design® software that offers a high degree of flexibility and is particularly recommended for highly interconnected processes as the GPPs, as also detailed by previous works on GPP simulation [12,13,26]. Hence, since our purpose is to compare different plant configurations in terms of the net produced energy and pollutant emitted, understanding how each unit operation is affecting the performance of the plant becomes crucial. First, the actual considered GPP, specifically the configuration related to Group 1 of

BG4 (20 MWe), has been implemented. This is a necessary step to check if the model is developed correctly since a direct comparison with real plant measurements can be performed. Subsequently, such a model has been adapted to represent the alternative configurations studied.

3.1. Conceptual model of the actual GPP

According to Fig. 1, few modeling assumptions deserve to be explained. Firstly, both the turbine expanding the geothermal fluid and the handling pump that circulates the hot water from the condenser to the cooling tower, are simulated at constant efficiency. The two streams exiting the condenser are not in thermal equilibrium, hence this operation is schematized with a series of different flash tanks, to separate the two-phase streams, and heat exchangers in which the energy transfer happens. The extraction of the NCG stream exiting the condenser is simulated by two constant efficiency compressors, between which the cooling operated by a water stream recycled from the evaporative towers is simulated in a flash tank. The AMIS® has been considered divided into two parts: a "black box" that knocks down the Hg flow rate with a constant efficiency, and a second section in which the oxidation of H_2S to SO_2 and the sequent abatement of the latter in a water absorption tower happen. Hence, three streams exit the AMIS®; the first one contains the abated Hg, while the other ones are the outputs of the C-2: the residual gas is sent to the evaporative towers while the residual liquid is recycled to the direct-contact condenser. Finally, the cooling system is simulated with a multi-stage equilibrium absorption tower with constant efficiency.

3.2. Considerations on alternative configurations

When simulating alternative system configurations, some other conceptual differences with respect to the one underlined in Section 3.1 have to be highlighted.

Firstly, the inlet conditions of the geothermal fluid are equal for all the simulated configurations and taken from the one in the BG4 model: this is done to analyze the offsets between the different configurations. Furthermore, where present, also the turbine discharge pressure, which represents the condenser pressure, was also taken equal to that of the measured one. We underline how, if in operative conditions this is a check parameter, in the simulation, it has been considered as independent and therefore to be specified. This lets us analyze the emissions in the atmosphere and energy consumption by excluding the variability of the conditions of the well.

When using surface condensers we need to consider that the geothermal vapor to be cooled down contains a certain amount of NCG, hence the condensation process is not isothermal. Furthermore, simulating the condensation by heat exchange instead of by direct contact requires modeling the surface condenser in two parts: a standard heat exchanger in which, to minimize the pressure drops, the geothermal steam passes through the shell side to be cooled down, and a flash separator that simulates the venting of NCG in a real condenser. In addition, since these two unit operations simulate one equipment, mixing the two-phase stream in transit between the two with external ones is not considered possible. We also underline that the condensation in surface condensers occurs in equilibrium between the liquid and the vapor phases, therefore, the gas sub-cooling is considered only when modeling direct-contact condensers.

Finally, the dry tower complex substituting the evaporative towers of the BG4 model, is represented by one air exchanger working at constant volumetric air flow and with only one constant rotation fan. Such a choice is justified since all the fans of the dry tower complex considered, contribute equally to the electrical power consumption.

3.3. Thermodynamic correlation and reactive aspects

The choice of the thermodynamic correlation sets the baseline for a meaningful representation of the real process in the simulation environment; in particular, stream compositions, unit operations, and operating conditions play a key role in this decision. Water and a NCG fraction are the main components of the geothermal fluid and the process streams in the GPP, while temperature and pressure undergo a strong variability (25 °C–200 °C and 0.08 bara-20 bara). For this reason, an Equation of State (EOS) model is considered the most adequate, and among all the EOS thermodynamic packages offered by UniSim Design® R460, the Peng–Robinson (PR) has been selected.

Since the model must reproduce the emissions of mercury (Hg), hydrogen sulfide (H_2S), ammonia (NH_3), and sulfur dioxide (SO_2), the thermodynamic correlations linked to such components have been checked, and eventually, refined so that their liquid/vapor balance is adequately managed. Specifically, the correlations for Hg and H_2S are taken from [12] in which a complete refinement procedure can be found. The NH_3-H_2O and SO_2-H_2O interactions are well-studied equilibria in the petrochemical industry and thus already included with a temperature non dependence by the PR package that has been specifically developed in such a sector. Lastly, the PR set does not consider the equilibria of ionic species in the aqueous solution, and, therefore, aspects related to pH changes cannot be modeled without the additional considerations explained below.

3.3.1. Hydrogen sulfide (H_2S) abatement

As anticipated, the AMIS® system has been schematized in different unit operations that require the introduction of reactive aspects. To reduce the atmospheric emissions of H_2S, also SO_2 has to be included in the model to correctly simulate the abatement which is performed through catalytic oxidation according to the reaction:

$$H_2S + \frac{3}{2}O_2 \rightleftharpoons SO_2 + H_2O$$

After removing Hg the remaining gas is initially added with compressed process air to ensure the oxygen necessary for the reaction (about 4% v/v) and then preheated inside the shell of an exchanger to reach the temperature necessary for the initiation of the oxidation reaction (≈220–240 °C). Subsequently, the catalytic oxidation reaction takes place inside a fixed bed adiabatic reactor. The reaction is exothermic and the heat generated is recovered through a shell and tube exchanger by preheating the reactor feed (see the scheme illustrated in [32, Figure 3].) The reaction takes place on a catalyst (usually TiO2 activated with calcium) with a complex pattern of oxidation and electron exchange between sulfur and oxygen, and its yield is displayed in [33, Figure 5]. The conditions to be considered when modeling this reactor are in the range 2000–2100 K^{-1}, that is, the oxidation yield is practically unitary. From these considerations, a conversion reaction is chosen to represent the H_2S oxidation, and its percentage yield in the simulator is expressed by (1).

$$\eta(\%) = C_0 + C_1 T + C_2 T^2 \quad (1)$$

T is expressed in [K] and the reference component for the conversion is H_2S. Given the catalytic nature of the reaction and the behavior of its yield with temperature, the chosen parameters are $C_0 = 99.0$, $C_1 = C_2 = 0$.

3.3.2. Sulfur dioxide (SO_2) abatement

The removal of SO_2 is performed by absorption in the liquid phase through the reaction:

$$SO_2\,(gas) + H_2O\,(liq) \rightleftharpoons H_2SO_3\,(liq)$$

The absorption of SO_2 produced by the catalytic oxidation of H_2S, occurs within the absorption column C-2 in which the gas comes into contact, through a counter-current flow, with cold water coming from the cooling tower [32, Figure 3]. The efficiency of this process essentially depends on the temperature inside the column, which should be indicatively lower than 35 °C, and the output pH from the column, indicatively higher than 4.5. If the geothermal water does not contain

sufficient dissolved NH_3, this pH value is achieved by adding NaOH to the process. Different water-soluble chemicals such as sulfites, sulfates, thiosulfates, and other sulfur species, are obtained as products of the sulfur dioxide removal reaction.

As mentioned in Section 3.3, chemical equilibria in solution and the pH, are not simulated with chosen PR package, thus the following procedure has been developed. Exiting the AMIS®, the purified gas is sent to the cooling tower, while the water acidified from the SO_2 absorption process is sent to the condenser (cold water). This favors the breakdown of H_2S towards the NCG stream, as its solubility in water decreases with the decreasing of water pH.

The modeling approach of the column consists of introducing a hypothetical component (*Hypo Component* in UniSim) which has the molecular weight of ammonium sulfite $(NH_4)_2SO_3$, thus following its formation reaction directly from SO_2 and NH_3. In other words, if the real formation reaction is an equilibrium described as follows:

$$H_2SO_3\,(liq) + NH_4OH\,(liq) \rightleftharpoons (NH_4)_2SO_3\,(liq) + H_2O\,(liq)$$

the one implemented in the simulator is a conversion reaction described by:

$$SO_2\,(gas) + 2\,NH_3\,(gas) \longrightarrow (NH_4)_2SO_3\,(liq) + H_2O\,(liq)$$

Whereas the C-2 column completely abates all the SO_2 that enters it, the reaction kinetics is considered to have as base component SO_2, and a quasi-unitary yield, with a small temperature-dependent component to keep its conversion more or less constant. The reaction kinetics parameter showed in (1) are set as follows: $C_0 = 99.0$, $C_1 = 0.1$, $C_2 = 0$. The term C_1 is defined positive, as experimental tests have verified that the absorption of SO_2 in NH_3 solution increases with temperature [34]. On the other hand, when temperature increases, the solubility equilibrium of SO_2 in the liquid solution is lowered, but the diffusion capacity of SO_2 molecules increases and so does the mass transfer. Furthermore, the temperature increase also accelerates the reaction due to the greater quantity of molecules activated [34].

3.3.3. Hypo Component $(NH_4)_2SO_3$ definition

The hypothetical component that represents $(NH_4)_2SO_3$ is defined in the software by first assigning a class/family to which the compound belongs. Being $(NH_4)_2SO_3$ a salt, the generic class named *Miscellaneous* is chosen, and to calculate its physical properties, the minimum knowledge required consists of molecular weight, and one between Normal Boiling Point and Ideal Liquid Density; the rest of the properties can be estimated from this couple. In the specific case, the molecular weight is the one of $(NH_4)_2SO_3$ (116.1 kg/kmol), while the normal boiling point is set to be very high (300 °C), as the component must remain in the liquid phase. A density close to the water one (800 kg/m^3) and a very high critical temperature (350 °C) have been also specified, to make sure that whereas this component goes into the gaseous phase, it is always possible to liquefy it. Finally, the interaction $(NH_4)_2SO_3$-H_2O is set identical to that of NH_3-H_2O.

3.4. Implementation of the base simulation model

In this section, the development of the model of BG4 using UniSim Design® (version R460) and different real data sources from EGP is described (Fig. 2).

On the other hand, Table 1 shows the measurements performed by EGP and the corresponding quantities in the model in Fig. 2, while Table 2 shows the conditions and composition of the geothermal fluid simulated.

With respect to the process diagram in Fig. 1, three main conceptual changes have been applied to simplify the model implementation. As anticipated, the condenser, is represented by several units to better simulate the temperature difference existing between the gaseous stream extracted by the compressor and the liquid stream sent to the pumping system. The first unit is a flash tank (in Fig. 2 referred to as *FirstSep*)

Table 1
Measurements performed by EGP and corresponding quantities of the BG4 model.

Stream in Fig. 2	Parameter measured
1	*T*, *P*, *F* [kg/h], composition
2	*P*
11	*P*
14	*P*
32	*F* [Nm^3/s]
10	*T*
16	*T*
17	*T*

Table 2
Geothermal fluid composition and conditions as it is simulated into the model (*Stream 1*).

Quantity	Value
Mass Flow [kg/s]	38.95
Temperature [°C]	208.0
Pressure [kPa]	1877
Molecular Weight	18.76
Mass Density [kg/m^3]	9.588
Mass Enthalpy [kJ/kg]	$-1.278\cdot10^{4}$
H_2O Mass Fraction	$9.272\cdot10^{-1}$
H_2S Mass Fraction	$1.127\cdot10^{-3}$
H_2 Mass Fraction	$5.955\cdot10^{-5}$
HCl Mass Fraction	0.000
Hg Mass Fraction	$5.999\cdot10^{-8}$
NH_3 Mass Fraction	$1.548\cdot10^{-3}$
CH_4 Mass Fraction	$1.989\cdot10^{-3}$
CO_2 Mass Fraction	$6.785\cdot10^{-2}$
N_2 Mass Fraction	$2.505\cdot10^{-4}$
O_2 Mass Fraction	$1.053\cdot10^{-5}$

which separates the liquid phase from the gaseous one of the turbine output stream. The gas phase first undergoes a fictitious cooling, without pressure drops, up to a temperature regulated by a logical operator (in Fig. 2 indicated as *ADJ-DT*). The cooled stream is then mixed with the recirculating liquid streams and sent to a second flash separator (in Fig. 2 indicated as *DirectContactCond*). The gas phase coming out of this second flash goes towards the gas extractor, while the liquid phase undergoes fictitious heating and is then mixed with the liquid stream from *FirstSep*. The purpose of the logical operator *ADJ-DT* is to vary the temperature of stream *5* until the temperature difference between the heated liquid exiting *E-102* (in Fig. 2 indicated as *10*) and the input stream to *DirectContactCond* (in Fig. 2 indicated as *6b*) is about 4 °C. The temperature of *10* is imposed from EGP documents. Secondly, the AMIS® is schematized using four unit operations: a component splitter (*AMIS_Unit* in Fig. 2), which briefly represents the Hg abatement plant with efficiency taken from EGP documents; a heat recovery unit (in Fig. 2 indicated as *E-1*) heats the reactant gaseous stream exploiting the hot gas stream reacted; a conversion reactor (in Fig. 2 indicated as *R-2*) in which the catalytic oxidation of H_2S to SO_2 takes place; and a flash tank (in Fig. 2 indicated as *C-2*) into which the cooled gas stream leaving *E-1* and part of the excess water from the evaporative towers converge. In all flash tanks present in the model (except for the initial separator *FirstSep*), the reaction between SO_2 and NH_3 also takes place to form $(NH_4)_2SO_3$. The outgoing liquid stream is sent to the condenser system, while the gaseous one mixes with the liquid stream inlet to the evaporative tower complex. Lastly, the cooling tower complex is schematized as a single absorption column (*Tower* in Fig. 2): the main purpose is to be more conservative in estimating the concentrations of Hg, H_2S, NH_3, and SO_2 leaving it. Since the simulation software lacks an evaporative tower model, the absorption column unit operation has been chosen, that is, the input–output scheme of such operation, a liquid inlet at the top and a steam inlet at the bottom, it is sufficiently close to the real one.

In addition, some other model simplifications are now detailed. The adiabatic (or isentropic) efficiency for the unit operation *Turbine*

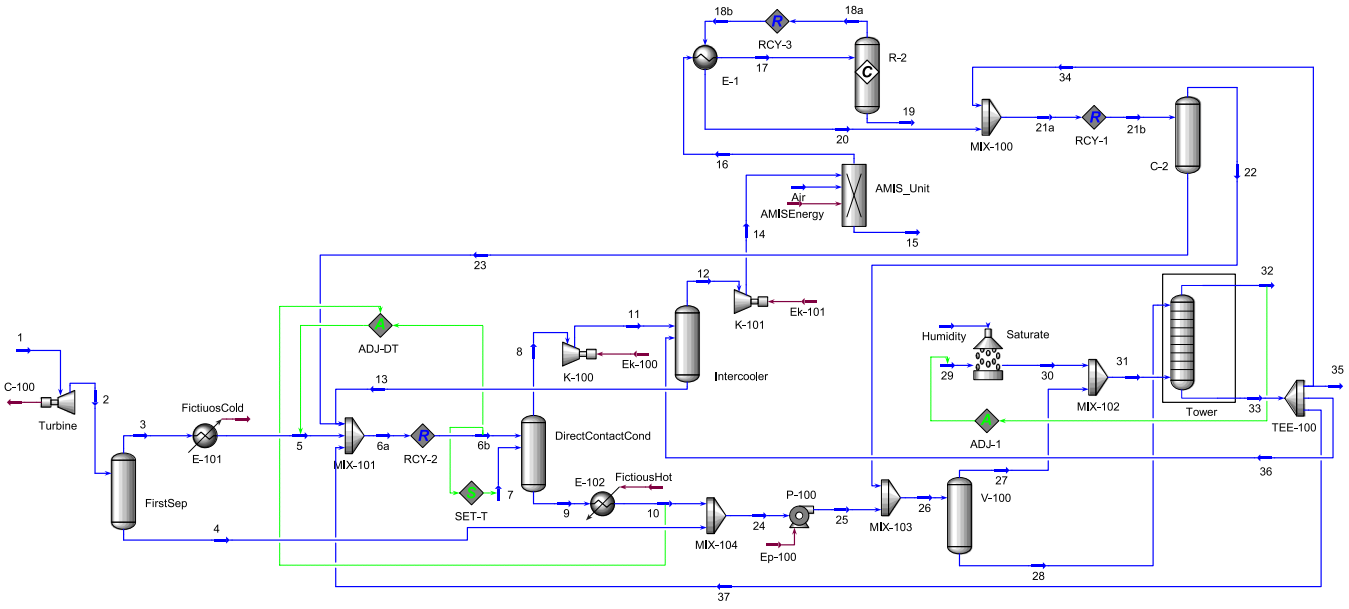

Fig. 2. PFD of the geothermal power plant BG4.

is set with an iterative procedure: its value is adjusted so that the produced mechanical power calculated in the simulation, multiplied by a mechanical/electrical conversion factor equal to 0.9, is as close as possible to the electric one reported in EGP documents. Therefore, the final value used in the simulation model is 76%. The efficiencies of both compressors *K-100* and *K-101* are used to tune the model for its calibration as detailed in Section 3.5, and the standard value of 80% is taken as their initial value, while the adiabatic efficiency of the handling pump *P-100*, has been set equal to 90%. As reported by EGP, the abatement efficiency of Hg is achieved by setting a split parameter in the unit operation *AMIS_Unit* equal to 97.8% by mass with respect to stream *14* exiting the gas extractor. In addition, to best simulate the dilution of the NCG stream with air to promote the oxidation of H_2S, another airflow is inserted into the *AMIS_Unit* (*Air* in Fig. 2). Mass flow rate, temperature, pressure, and relative humidity of such stream are strictly linked to the dataset used for the model reconciliation, hence, their values have to be defined accordingly.

The split values of *TEE-100* are computed using a spreadsheet operation in which the mass fractions of the streams *34, 35, 36*, and *37* are calculated. The flow rates of the first three streams (two of the water recycles and the re-injection one) are taken from EGP documents while the latter one is extrapolated from the assumption that the liquid stream leaving the tower (*33* in Fig. 2) has approximately the same mass flow as the inlet one. Consequently, the split ratios for each stream are evaluated and used as initial reference values for the data reconciliation procedure in Section 3.5.

As already underlined in Section 3.3, using the PR thermodynamic set is not possible to model the equilibria in the ionic phase. Given that, it is necessary to find an alternative method to reduce the emissions of NH_3 from the cooling tower and therefore make the simulated model closer to the industrial reality. One operative practice used at the level of the direct-contact condenser to lower the pH of the solution, so to enforce the NH_3 absorption into the liquid phase, is to inject sulfuric acid into the equipment. To simulate such practice, a fictitious stream of pure gaseous SO_2 (in Fig. 2 named *7*) is introduced into the *DirectContactCond* tank. The temperature of such a stream is set identical to the one of the mixture entering the tank, through the logic unitary operation *SET-T*. The mass flow of *7* is calculated by the spreadsheet *pH-control* in the following way. The real volumetric flow of H2SO4, taken from EGP documents, is converted into molar flow considering the liquid density at normal conditions (1830 kg/m^3). Hence, the fictitious mass flow of SO_2 is calculated from its molar flow imposed equal to the molar flow of H2SO4. Another aspect linked to equilibria in the ionic phase involves the SO_2 absorption into water. In the real case scenario, in the C-2 column at the end of the AMIS®, all the gaseous SO_2 produced by the oxidation of H_2S is absorbed in the liquid phase. However, in the simulated model, the practical way to abate the SO_2 is to convert it into $(NH_4)_2SO_3$, but the amount of NH_3 in the aqueous stream coming from the evaporative tower complex is not sufficient, which therefore gives in output from *C-2* still a high quantity of unreacted SO_2. For this reason, a reactive flash tank (in Fig. 2 named *V-100*) is added to mix the gaseous stream coming from *C-2*, rich in SO_2, and the liquid stream sent to the tower, rich in NH_3, so to encourage the total conversion to $(NH_4)_2SO_3$. The role of *V-100* is therefore to complete the absorption of SO_2 which, in reality, happens entirely in column C-2. Finally, the gas stream exiting this tank is mixed with *30* and sent to the bottom of *Tower*, while the liquid one at its top.

Finally, two additional logic unit operations have been included in the model. The unit operation *Adjust* (ADJ-1 in Fig. 2) sets (indirectly) the volumetric flow rate of *32* to a setpoint value, taken from EGP data, i.e. 3931887 Nm^3/s, by varying the mass flow rate of the air stream *29*. The relative humidity of the air stream *30* entering the evaporative tower, is set by adding a fictitious water stream (*Humidity*) to the dry air stream *29* via the unit operation *Saturate*. So, as for the additional air stream in the *AMIS_Unit*, the environmental conditions used for the tower air are those representing the situation from which the other data of the model are extracted.

The second logic unit operation used is *Recycle* (RCY-1, RCY-2, and RCY-3 in Fig. 2). RCY-1 and RCY-3 are in the AMIS®section, at the input to the flash tank *C-2*, and at the input of the oxidation reactor *R-2*, while RCY-2 is at the input to the central part of the condensing system. The three recycling blocks, and thus the three fictitious streams, allow the simulator to perform cyclic calculations, guaranteeing the model efficiency.

3.5. Data reconciliation

The optimization variables used for reconciling the available data, are the following:

- N_S: number of *Tower* stages
- η_S: *Tower* stage efficiency
- η_K: *K-100* and *K-101* efficiencies, gas extractor compression stages

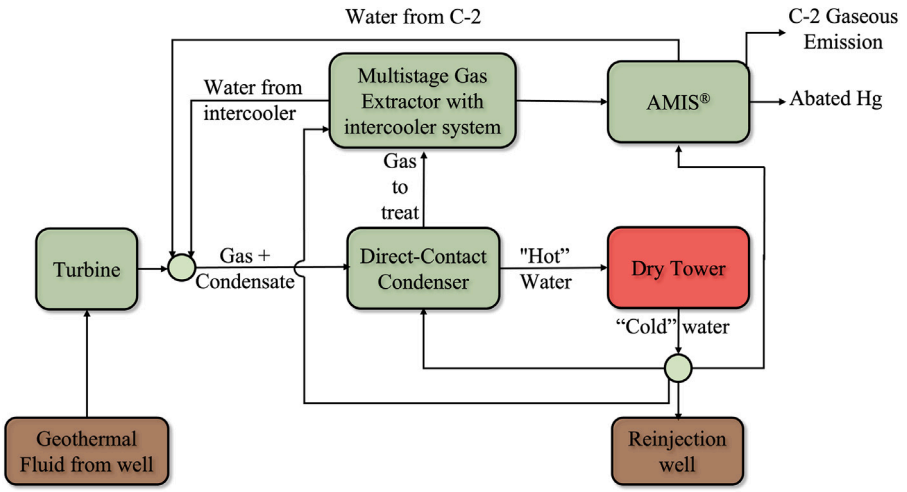

Fig. 3. PFD of the geothermal power plant alternative configuration DCDry.

- $\xi_{TEE,i}$: split parameters in *TEE-100*

The values $\xi_{TEE,i}$ multiply the mass flow of the stream entering the splitter (*33*) to obtain the ith mass flow of the output streams.

The objective function Φ used for the data reconciliation procedure is based on the errors between measured ($\bar{\phi}_i$) and predicted model (ϕ_i) values of selected key quantities. The quantities taken in considerations are temperature of streams *28* and *37*, volumetric flow rate of streams *14, 28, 34, 36*, and pollutants (Hg, H_2S, NH_3) mass flow rate of streams *14* and *32*. The various terms of the objective function have all been normalized in the following way:

$$\Phi = \sum_{i=1}^{12} \left| \frac{\phi_i - \bar{\phi}_i}{\bar{\phi}_i} \right| \tag{2}$$

Varying N_S, different runs of the following optimization problem have been executed to find the optimal combination of variables values:

$$\min_x \Phi(x) \tag{3}$$

subject to

$$x_{\min} \leq x \leq x_{\max} \tag{4}$$

in which $x = [\eta_S; \eta_K; \xi_{TEE}]$, $x_{\min} = [5; 60; 0]$, and $x_{\max} = [100; 95; 1]$. The optimization problem (3) is solved using the *Optimizer* tool available in UniSim Design® and selecting the Sequential Quadratic Programming (SQP) algorithm [35] as solver.

3.6. Results

To have a wider view of the seasonal change that the GPP operating conditions encounter, and thus have a more reliable simulation model, two different sets of environmental conditions have been tested in the data reconciliation: the first named "*winter*" conditions, and the second one "*summer*" conditions. The two conditions refer to different EGP documents in which the air characteristics are 9 °C, 110 kPa, and 80% relative humidity for "*winter*" and 23 °C, 110 kPa, and 58% relative humidity for "*summer*". Since the computational cost of such a problem is considerable due to its high non-linearity and the complexity of the simulation model, different tests have been performed by varying the starting point of the iterations. The values that led to a nearly-global minimum are reported in Table 3.

The results reported in Table 4 are the best ones obtained, for matching the EGP measured data and obtaining a conservative model on the emission side in both conditions tested. The emissions of H_2S for the *winter* conditions and Hg for the *summer* ones are the only two flow rates smaller than the measured values, albeit comparable to them in terms of order of magnitude (8% and 11%, respectively). In addition, the NH_3 emissions exceed the measurements by 15% and by 28%, while the SO_2 emission flow rate is null as it is removed all within the GPP process. We underline that this GPP model has been calibrated not only to, when possible, conservatively estimate the gaseous emissions but mainly to represent the base asset to compare alternative configurations both from an emissive and an energetic point of view.

For completeness, the Heat and Material Balance for the BG4 model in both the "*winter*" and the "*summer*" conditions are provided in Section A of the Supplementary Information (SI).

Table 3
Optimal values obtained with data reconciliation of the BG4 model.

Quantity	Initial value	Optimal value
η_S [%]	75	35.5
η_{K-100} [%]	80	90
η_{K-101} [%]	80	80
$\xi_{TEE,37}$	0.893	0.878
$\xi_{TEE,34}$	0.068	0.076
$\xi_{TEE,36}$	0.029	0.031
N_S	5	3

4. Alternative configurations

In this section the different alternative configurations of the BG4 model built and reconciliated in Section 3.4 are presented.

4.1. Direct-contact condenser and dry towers (DCDry)

A PFD of the simulated process DCDry is shown in Fig. 3. With respect to the BG4 model, the following aspects should be highlighted. The fictitious flow of SO_2 in the condenser has been set to zero, as with this configuration, not enough NH_3 is able to reach the AMIS®. The air fan (in Fig. 3 named *Dry Tower*) which simulates the complex of dry towers, has been dimensioned by setting the temperature of the outlet stream to 27.3 °C. This value and the other sizing parameters are taken from benchmark data of dry towers and reported in Table 5. The pressure drops on the process flow side have been set to 50 kPa. The temperature of the air entering the fan is equal to 9 °C since the reference weather conditions for the implementation of DCDry are the *winter* ones. The air flow rate has been selected so that no temperature crossing takes place into the tower, and therefore its actual value has been set to $10^7 m^3/h$. The splitting values of the liquid streams exiting the tower have been set so that the resulting volumetric flow rates were as close as possible to the values indicated by EGP.

Table 4
Values of the monitored variables obtained after data reconciliation for BG4 basic model in *winter* and *summer* conditions, compared with the corresponding EGP measured data.

	Quantity	*Winter*			*Summer*		
		Measured	Simulation	Δ[%]	Measured	Simulation	Δ[%]
Emission	$F_{H_2S,32}$ [kg/h]	8.3	7.67	7.59%	7.61	9.36	23.00%
	$F_{NH_3,32}$ [kg/h]	17.7	20.3	14.69%	26.5	33.9	27.92%
	$F_{Hg,32}$ [g/h]	0.6	0.66	10.00%	0.9	0.8	11.11%
	$F_{SO_2,32}$ [kg/h]	–	0	–	–	0	–
To AMIS	$F_{H_2S,14}$ [kg/h]	131.63	151.95	15.44%	148.33	150.24	1.29%
	$F_{NH_3,14}$ [kg/h]	0.001	1.94	> 100%	0.00126	1.44	>100%
	$F_{Hg,14}$ [g/h]	5.48	7.93	44.71%	8.7	7.78	10.57%
	F_{14} [kg/h]	12200	13028	6.79%	11800	12421	5.26%
Water	T_{28} [°C]	34	34.53	1.56%	37.3	37.37	0.19%
	F_{28} [m^3/h]	4500	4468	0.71%	4450	4688	5.35%
	T_{37} [°C]	20.7	20.84	0.68%	24.4	25.58	4.84%
	F_{36} [m^3/h]	133	136.5	2.63%	184	173	5.98%
	F_{34} [m^3/h]	320	334.6	4.56%	380	366.7	3.50%

Table 5
Design parameters of the selected dry tower.

Variable	Symbol	Value	Unit
Single Cell Area	A_{cell}	586	m^2
Design Wind Velocity	v_w	3	m/s
Number of cells	N_{cell}	10	–
Air Inlet temperature	$T_{air,in}$	22.3	°C
Heat Rejected	$Potw_{th}$	70.7	MW$_{th}$
Warm water temperature	$T_{H_2O,in}$	36	°C
Cold water temperature	$T_{H_2O,out}$	27.3	°C
Total fan power at motor terminals	$Potw_m$	1300	kWe

Table 6
AMIS® plant input stream characteristics in the 5 simulated configurations (*winter* conditions).

Flow rate	BG4	DCDry	SDry	SWet	ORCDry
H_2S [kg/h]	151.95	157.69	157.93	157.11	115.1
NH_3 [kg/h]	1.94	44.61	135.04	6.65	2.65
Hg [g/h]	7.93	8.46	8.4	8.34	6.93
Total [kg/h]	13028	12757	14822	11882	9106

It is important to note that in this setting the emission occurs directly from the C-2 column in the AMIS® plant and therefore the flow of H_2S emitted derives entirely from the stripping of the liquid stream coming from the dry towers. Furthermore, the consistent emission of SO_2 can be justified by the $(NH_4)_2SO_3$ formation reaction: in this setting, the NH_3, mainly present in the water coming from the dry tower, is the limiting reagent. Since there are no other possibilities of reaction with "new" NH_3, the SO_2 not absorbed in the liquid and not reacted is found directly as a gaseous emission. The complete Heat and Material Balance for configuration DCDry is reported in Section B of the SI. Analyzing the balance we underline the discrepancy in flow rates between the gas stream exiting the condenser and the one entering the AMIS®; this is due to the quantity of water condensed in the intermediate cooling between the two compression stages. On the contrary, the flow rate of NCG, such as CO_2, remains essentially the same.

4.2. Surface condenser and dry towers (SDry)

A PFD of the simulated process SDry is shown in Fig. 4. For the sake of comparison, the air fan *DryCooler* in Fig. 4 has been dimensioned as in configuration DCDry in Section 4.1. The direct-contact condensers in BG4 and DCDry models, have been replaced by surface condensers, each one broken down into two parts, as explained in Section 3.2. The heat exchanger which cools the process stream with a cold utility has been modeled with a "*Weighted*" design, available in the simulator in the case of mixtures with phase change, as in the case of interest. The sizing has been done by imposing as a specification a minimum delta *T* approach equal to 15 °C between two streams. The pressure drops imposed are 50 kPa on the tube side for the cold utility and 0.4 kPa on the shell side for the geothermal fluid. The second part of the condenser is a flash separator which divides the gas stream from the liquid stream condensed in the exchanger. The cold utility circuit consists of water with a flow rate of 6900 m^3/h in which, 95.5% of the total is sent to the main condenser while the rest is sent to the intercooler between the two gas extractor stages. The liquid stream leaving the surface condenser is pumped directly to the head of column *C-2* in which the reaction of transformation of SO_2 into sulfite takes place. Both streams exiting the *C-2* leave the process, the gaseous one as emissions, and the liquid one is re-injected into the well. Then we underline that a fourth *Recycle* block in the cold utility water cycle has been introduced and placed in input to the Dry Tower for a matter of numerical efficiency of the simulation. Results show how the emission of H_2S is quite low and this is mainly because although the concentration in the water coming from the tower is greater, the flow rate of the latter is about half of the one in the DCDry setting. Consequently, the H_2S flow rate is also much lower, because most of it tends to pass through the AMIS® and, therefore, be oxidized. In addition, it should be emphasized that all the results for the SDry setting are strongly affected by the operating conditions used, in particular by the turbine discharge pressure. Variations of tens of Pascal are enough to significantly shift the balances of condensation. In addition to this, the surface condenser does not provide for a sub-cooling, and the gaseous stream is therefore in thermal equilibrium with the liquid one leaving the equipment. Table 6 also shows a consistent flow rate of NH_3 entering the AMIS® plant, and this is mainly for two reasons. The first one is that the temperature of the gases exiting the condenser is too high because the cold water temperature is not lower than 27.3 °C (parameter imposed by the design of the dry tower), compared to about 24 °C of the water exiting the wet tower in BG4. Secondly, the surface equipment is unable to pull the vacuum like the corresponding direct-contact unit. Hence, setting the turbine exhaust pressure, and, therefore, the working pressure of the condenser, equal to the one in the other configurations where there is a direct-contact mixing results in bad environmental performance. Therefore, an increase in the turbine exhaust pressure has been considered at the expense of energy production. On the other hand, further consideration regarding this evidence should be made with respect to the energy analysis. In general, using the working pressure as in BG4 model, the gas flow rate that leaves the condenser is very high (about 43 t/h). This induces a high consumption of the compressors of the gas extractor group as well as the practical inability of treating such a flow rate. Vice versa, the very low liquid flow out of the condenser causes a practically negligible electrical consumption for the circulation pump. It is therefore clear that the entire energy balance of SDry can be modified by acting on the condenser and thus making it comparable

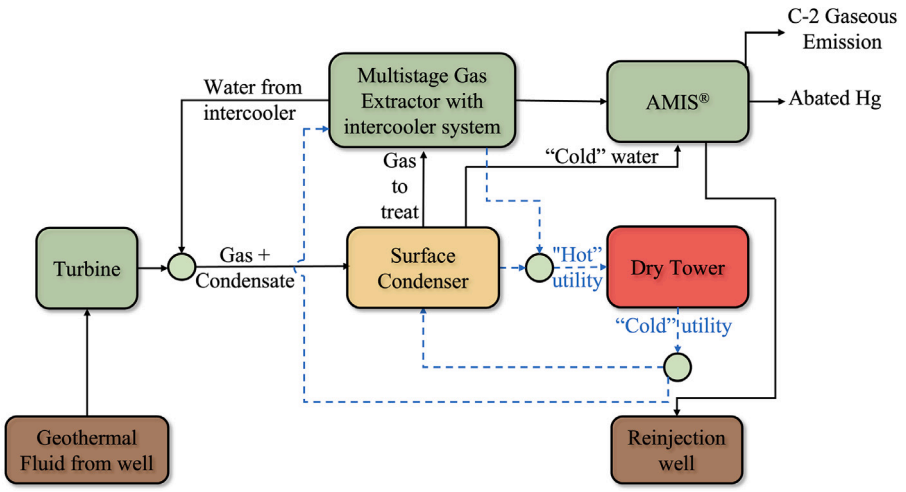

Fig. 4. PFD of the geothermal power plant alternative configuration SDry. The blue dashed lines indicate the separate circuit for the cold utility.

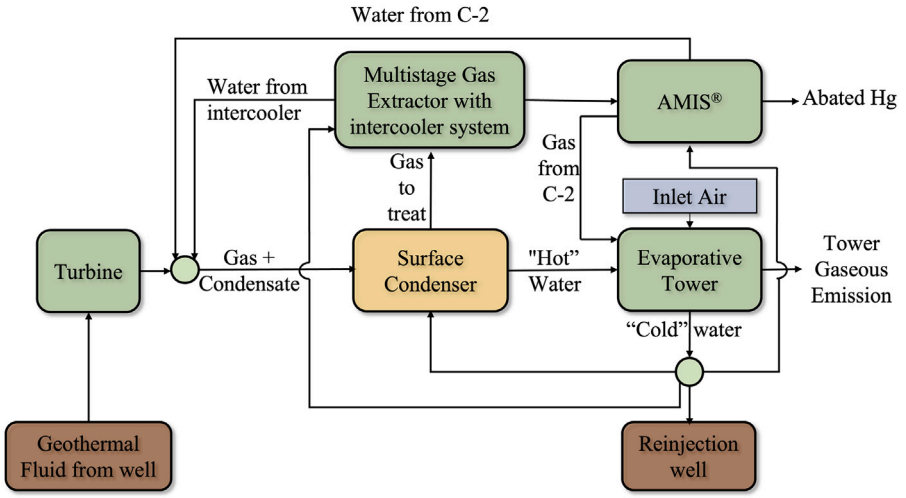

Fig. 5. PFD of the geothermal power plant alternative configuration SWet.

with that of the other configurations. Given the above considerations, it is necessary to revise the hypotheses made previously in Section 3.2, and, in particular, the turbine exhaust pressure is set to 8.237 kPa. Since when slightly raising the working pressure of the condenser the environmental performance has considerably improved, the results produced with these modifications are the ones compared with the other configurations (see Table 6). The complete Heat and Material Balance for SDry is shown in Section C of the SI.

4.3. Surface condenser and wet towers (SWet)

A PFD of the simulated process SWet is shown in Fig. 5. With respect to the basic configuration BG4, the only change that should be highlighted in the SWet setting is the replacement of the direct-contact condenser with a surface condenser. As already seen for the configuration SDry, the condenser is split into two parts, but in this case the heat exchanger has been dimensioned with a minimum delta T approach equal to 5 °C. Once out of the separator, the two liquid streams exiting the condenser are mixed together and pumped at atmospheric pressure to the evaporative tower, in analogy with the basic setup BG4. The air flow entering the evaporative tower has been adjusted using an *Adjust* block as seen for the BG4 model. Both the air characteristics and the target flow rate of the emitted gas have been taken from the *winter* conditions references. It is emphasized that in this case, unlike the BG4 model, there is a high emission of NH_3. This is because in the surface condenser there is no injection of acid for neutralization, as it is in the direct-contact unit. An assessment of whether and where to acidify the stream could be relevant for emissions purposes. Moreover another aspect to take into consideration is the fouling problem in the heat exchanger. As a matter of fact, in this case, the fluid in the tube side is still the geothermal water exiting the wet tower and not the cold utility as in the SDry configuration, with a consequent cost increase in equipment maintenance. The complete Heat and Material Balance for SWet is shown in Section D of the SI.

4.4. Organic Rankine Cycle (ORCDry)

A PFD of the simulated process ORCDry is shown in Fig. 6. It is to be underlined that differing from normal binary cycles in which the geothermal fluid contains a limited content of non-condensable gas (<0.5%–1%), the one considered (see Table 2) does need an abatement system to avoid working at very high pressures. Therefore, according to the scheme proposed by EGP on these considerations the simulated model is built as follows. The geothermal fluid enters a cooler which simulates the transfer of heat from the geothermal fluid to an Organic Rankine Cycle (ORC) for the production of electricity. This cooling takes place under pressure (1600 kPa) and lowers the fluid temperature up to 70 °C. The two-phase fluid enters a separator which

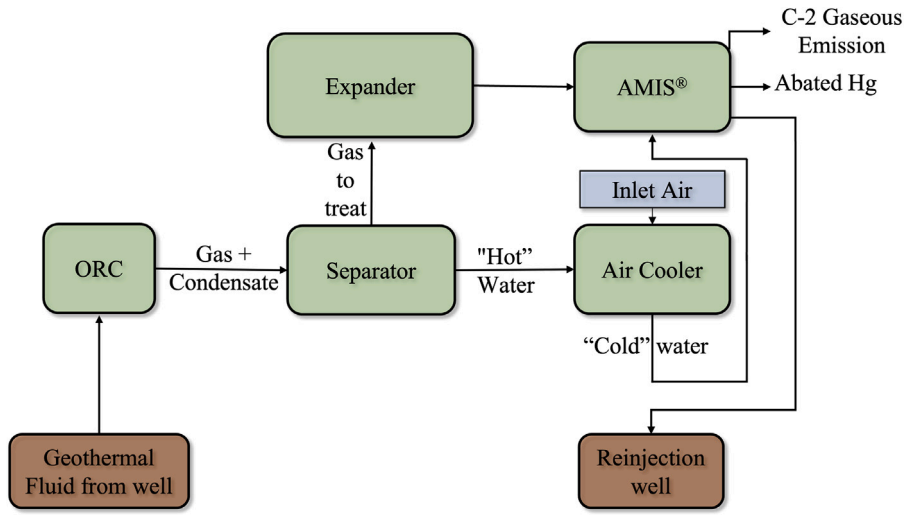

Fig. 6. PFD of the geothermal power plant alternative configuration ORCDry.

divides the gaseous stream from the liquid one. The gaseous current, mainly composed of NCG, goes towards an expander which brings it to atmospheric pressure, producing energy before entering the AMIS®. On the other hand, the liquid stream goes under pressure to an air cooler which cools the process stream to 30 °C. The pressure losses on the process side have been imposed equal to 100 kPa. The air inlet temperature to the fan is 9 °C as the reference conditions are still the *winter* ones. The air flow rate has been selected in such a way that there is no temperature crossing in the exchanger, and therefore imposed equal to $5 \cdot 10^5$ m^3/h (actual value). The liquid stream leaving the air cooler is pumped directly to the head of the C-2 column. Finally, as for configuration SDry, both streams exiting the C-2 separator leave the process, the gaseous one as emissions, and the liquid one is re-injected into the well.

This is definitely the configuration that most differs from the actual one, among all the alternatives analyzed. The ORC has not been explicitly simulated, but replaced by a heat exchanger that cools the geothermal fluid and lowers its pressure slightly. This is because, to study the emissions of pollutants into the atmosphere, it was not considered necessary to simulate the entire organic cycle. The heat generated in this exchanger corresponds to the heat acquired by the organic fluid (e.g. n-pentane) which then goes to expand in the turbine and generate electricity. Therefore, the electrical power actually generated by the ORC can be calculated simply from the thermal power obtained from the exchanger after appropriate conversion with energy efficiencies. The great quantity of H_2S emitted comes directly from the liquid side of the process and derives from the separation under pressure (see Table 6). Also, a great amount of NH_3 can be seen in the water but most of it is then consumed in the C-2 column to absorb SO_2. Finally, the complete Heat and Material Balance for ORCDry can be found in Section E of the SI.

4.5. Configuration comparison

To better compare the results obtained, Table 6 reports the flow rates of the pollutants of interest for this study in the input stream to the AMIS® plant, that is the part of the GPP common to all settings.

5. Results analysis

5.1. Energy performances

For a comparative study of the different simulated configurations, it is important to analyze the GPP performance in terms of net energy production and understand which one is more convenient. Hence, to best compare the results obtained, the contributions given by the various power producer/consumer components in the different configurations are reported in Table 7, for which some remarks and clarification are needed.

First, as explained in Section 4.4, the production of electricity in configuration ORCDry is carried out by the organic fluid in the ORC itself. Therefore the nature of the turbine is also different from the steam turbine used in the other configurations. Hence, the turbine power value shown in Table 7 is the electrical power calculated from the thermal power transferred by the geothermal fluid to the organic fluid of the ORC, as follows:

$$Pow_e = Pow_{th} \cdot \eta_{th2e} = 93.13 \cdot 0.23 = 21.42 \text{ MWe} \tag{5}$$

The efficiency η_{th2e} that converts the thermal (Pow_{th}) into electrical (Pow_e) power is conservatively calculated from the data and information contained in EGP documents.

Secondly, the powers consumed by the dry towers in DCDry and SDry and by the air fan in ORCDry are calculated from the thermal powers extracted from the simulator. Specifically, the electrical–thermal conversion efficiency is calculated as follows. From Table 5, in the reference setting, the fans consume 1300 kW for removing 70.7 MW_{th} of thermal power with an air inlet temperature of 22.3 °C, while the one used in the simulations is 9 °C for consistency with the *winter* conditions selected. This means that the air flow needed at 22.3 °C to cool down the process stream from 36 °C to 27.3 °C it is conservatively higher than the one used in the simulation. Ultimately, by calculating an efficiency equal to:

$$\eta_{DryCooler} = \frac{1.3 \text{ MW}_e}{70.7 \text{ MW}_{th}} = 0.0184 \tag{6}$$

the electric power consumption is obtained in the following way:

$$\begin{aligned} Pow_{e,DCDry} &= 57.12 \text{ MW}_{th} \cdot \eta_{DryCooler} = 1.051 \text{ MW}_e \\ Pow_{e,SDry} &= 73.20 \text{ MW}_{th} \cdot \eta_{DryCooler} = 1.346 \text{ MW}_e \end{aligned} \tag{7}$$

Making an approximate and conservative estimate, we can also consider the ORCDry fan with the same efficiency as the dry tower, therefore:

$$Pow_{e,ORCDry} = 6296 \text{ MW}_{th} \cdot \eta_{DryCooler} = 0.116 \text{ MW}_e \tag{8}$$

Lastly, the power consumption of the wet towers is converted into the power consumption of the fans. It should be considered, however, that it was not possible to directly calculate the power of the evaporative towers, due to the lack of reliable pressure loss data. In particular,

Table 7
Energy analysis of the various configurations. The typology indicates producer (P) or consumer (C). The quantities shown are all mechanical powers (at the axis) in MW. The quantities not directly obtained from simulation but calculated are detailed within the equations indicated.

Component	Typology	BG4	DCDry	SDry	SWet	ORCDry
Turbine	P	23.81	23.81	23.4	23.81	21.42 (5)
Compressor 1st stage	C	0.448	0.451	0.557	0.391	–
Compressor 2nd stage	C	0.719	0.798	1.059	0.688	–
Condenser water pump	C	0.185	0.674	0.004	0.019	–
Dry Tower	C	–	1.051 (7)	1.346 (7)	–	–
Water cycle pump	C	–	–	0.254	–	–
Expander	P	–	–	–	–	0.0917
Air Cooler	C	–	–	–	–	0.116 (8)
Wet Tower	C	0.450	–	–	0.450	–
Net Power		22.01	20.83	20.17	22.26	21.39

since the cooling tower was modeled as an absorption tower, it was not possible to calculate the power absorbed by the tower fans from the simulations, and, therefore, conservative considerations have been applied. From available EGP data and as stated in [12], the registered consumed power of the fans is quite steady varying the tower air flow in Nm^3/s, that is, the maximum shift around the mean value of consumption is a few percentage points. For this reason and to be conservative, the power consumption of the wet towers has been calculated using the nominal power of three cells: 150 kW·3 = 450 kW = 0.45 MW.

Hence, analyzing the results shown in Table 7, the best technical performance in terms of net electricity produced, is obtained for configuration BG4 and SWet, i.e those using the evaporative tower as a vent into the atmosphere. In addition, it would be necessary to deepen the study on the consumption of dry towers. Improvements in the sizing of such equipment that allow a decrease in the estimated power consumption, in fact, could become crucial and make configurations DCDry and SDry competitive from an energy point of view. In fact, if simple calculations are carried out based on the dry tower design data in Table 5, the following results can be obtained.

The nominal air flow to absorb 70.7 MWth at a temperature of 22.3 °C is equal to:

$$F_{air} = v_w \cdot A_{cell} \cdot N_{cell} = 3 \cdot 3600 \cdot 586 \cdot 10 = 6.33 \cdot 10^7 \ \mathrm{m^3/h} \tag{9}$$

By imposing the air flow F_{air} in the simulator, the following exchange coefficient is obtained: $UA^0 = 4.04 \cdot 10^7 \mathrm{kJ/(°Ch)}$. At this point, the head losses ΔP of the tower on the air side can be calculated as follows:

$$\Delta P = \frac{Pow_m}{F_{air}} = \frac{Pow_e \cdot \eta_{m2e}}{F_{air}} = \frac{1.3 \ \mathrm{MW_e} \cdot 0.85 \cdot 3600 \ \mathrm{s/h}}{6.33 \cdot 10^7 \ \mathrm{m^3/h}} = 0.063 \ \mathrm{kPa} \tag{10}$$

where η_{m2e} is the transformation efficiency from electricity to mechanical energy. Hence, by setting in the simulator the air temperature considered in Sections 3.6 and 4 and equal to 9 °C, the air flow rate was varied until the exchange coefficient calculated was as close as possible to the one obtained for the reference case (UA^0). Then, imposing an air flow rate equal to $F'_{air} = 1.015 \cdot 10^7 \mathrm{m^3/h}$ a global exchange coefficient equal to $UA' = 4.05 \cdot 10^7 \mathrm{kJ/(°Ch)}$ is obtained, with a deviation from the reference case of 0.2%. Considering the same pressure drops obtained from the nominal case and the same efficiency value, the consumed electric power is as follows:

$$Pow'_e = \frac{F'_{air} \cdot \Delta P}{\eta_{m2e}} = \frac{1.015 \cdot 10^7 \ \mathrm{m^3/h} \cdot 0.063 \ \mathrm{kPa}}{0.85} = 208.4 \ \mathrm{kW_e} \tag{11}$$

Finally, it can be seen how the power absorbed by the dry tower is very underestimated using this procedure, and also how the power itself varies significantly with the variation of the environmental parameters. It is therefore considered more conservative to use the procedure shown in Table 7.

Table 8
Environmental analysis of the various plant configurations analyzed. The reference stream is the emission into the atmosphere of the various configurations (wet tower or C-2 column), while Total Dry indicates the total dry flow rate (free of H_2O).

Flow rate	BG4	DCDry	SDry	SWet	ORCDry
H_2S [kg/h]	7.67	1.78	1.72	2.56	42.5
NH_3 [kg/h]	20.3	0	8.54	58.89	5.03
Hg [g/h]	0.66	0.94	0.185	0.26	2.5
SO_2 [kg/h]	0	7.19	0	0	0
CO_2 [kg/h]	9514.6	9514.9	9455.8	9507.9	9400.5
CH_4 [kg/h]	278.95	278.95	278.95	278.95	278.95
Total Dry [kg/h]	10653†	10628	10569	10666†	10612

5.2. Environmental performance (Emissive scenarios)

To fully compare the results obtained and evaluate the different emissive scenarios, Table 8 reports the atmospheric emissions of the pollutants considered in this study. Together with the one entering the AMIS®, this stream is common among all configurations and therefore can be taken as a reference for environmental performance comparison. We underline once more how the geothermal well considered is the same for all simulations, that is, the composition of the inlet stream is shared among all the modeled configurations. The gas flow rate for the configurations with wet towers, BG4 and SWet (identified with † in Table 8), has been calculated as the difference between the tower outlet gas and the tower inlet air streams, which values are fully reported in the corresponding section (see Sections A and D of the SI). The dry total is then obtained by removing H_2O from the resulting difference stream. From the analysis of Tables 6 and 8 different considerations can be stated. The amount of H_2S treated by the AMIS® is quite comparable in all 5 settings, except for ORCDry. As anticipated in Section 4.4, this is due to the high pressure (16 bar) at which the equipment that separates the gaseous stream, mainly composed of NCG, and the condensed phase operates. This leads to dissolving a large quantity of H_2S in the water which, by stripping in the C-2 column, is found in such large quantities in the emissive stream.

Regarding the NH_3, we underline how in the inlet stream to the AMIS® for DCDry there is a quantity of two orders of magnitude higher than the corresponding one of the actual configuration BG4. The reason is that with the use of the wet tower (BG4) the emission of NH_3 into the atmosphere is about 20 kg/h and this allows to have around 240 kg/h at the condenser inlet. Instead, when employing the dry tower (DCDry), the NH_3 is trapped in the process scheme because it is all consumed by SO_2. The consequence is that the quantity circulated to the condenser is much greater than in the actual case (about 2300 kg/h). Given this, the 44 kg/h entering the AMIS® recorded for DCDry configuration is linked to the 94 kg/h that leaves the condenser, representing approximately 4% of the NH_3 circulating in the water. Although both configurations SDry and SWet are equipped with a surface condenser, in SDry much more NH_3 reaches the AMIS®. As anticipated in Section 4.2, the temperature of the outlet gases from the condenser is governed by the cold water temperature which, in SDry setting, is not lower than 27.3 °C as

imposed by the dry tower design. Oppositely, the wet tower in SWet guarantees outlet water that is approximately 3 °C colder than the previous case. This difference influences the solubility of the substances in the condenser and results in a more significant transfer of NH_3 to the gas phase for SDry. In addition, another substantial difference is in the emissions of NH_3 between BG4 and SWet. In the latter, the amount of NH_3 emitted is about three times compared to the actual setup. This is mainly due to the use of the surface condenser and the consequent impossibility of introducing an acid stream directly into the equipment. In this specific case, an equivalent amount of SO_2 equal to 73 kg/h would be enough to reach the NH_3 emissions in the actual configuration. It should also be considered that the actual amount of sulfuric acid used for BG4 and reported in EGP data, converted into equivalent SO_2 is approximately 86 kg/h.

Configuration DCDry is the only one that presents a problem with the emission of SO_2. Precisely, for what has been said regarding the large quantities of NH_3 circulating in the plant water, the water stream used for washing the C-2 column, in this case, is approximately 230 m^3/h containing around 103 kg/h of NH_3. If we add these 103 kg/h to the 44 kg/h entering the AMIS®, a total of 148 kg/h of NH_3 has to neutralize about 294 kg/h of SO_2. This is the reason why in this case the NH_3 is the limiting reagent, and, therefore, SO_2 emissions can be found. The possibility of basifying the C-2 column should be considered in this case; in particular, in terms of stoichiometric NH_3, it would take 13.3 kg/h to completely break down the excess SO_2.

Additionally, all the scenarios analyzed emit a dry gaseous stream of equal flow, for the most part composed of all the CO_2 that enters the turbine from the well. Small differences in the flow rates of a numerical nature are generated by the solver used within the simulator, nonetheless, they still fall within the predetermined tolerances. CH_4 suffers a similar fate, which is all emitted as a gas, representing the second major component of the emissive current. Therefore, there are no obvious differences in the emissions of greenhouse gases among the various configurations.

Given the considerations made, the best result in terms of pollutant emission is obtained with two configurations. In DCDry the emission of SO_2 does not have the toxicity levels of H_2S and Hg and it can be controlled with a slight alkalinization of the C-2 column; while in SDry the modest emission of NH_3 can be eliminated with slight acidification of the C-2 column, maintaining emissions of H_2S and Hg are the lowest among all the configurations considered. It can be noted that although the ionic equilibria in the aqueous phase have not been considered, the methodologies implemented to simulate the acid–base reactions, and therefore better represent the distribution of the gaseous species as a function of the pH of the process waters, have always been conservative. As a matter of fact, when SO_2 emissions are present, those of NH_3 are not and vice versa, always representing the maximum deviation from standard conditions.

6. Conclusions

In a world always in need to find sustainable green energy sources, geothermal power plants (GPPs) represent well-established possible solutions to such a dilemma. Nevertheless, as with all energy production activities, also GPP is not free from producing environmental impacts, especially during the operational phase with the emission of non-condensable gases (NCG). Life-cycle assessment (LCA) studies on GPPs have shown the importance of primary data to build inventories and perform reliable analyses. On the other hand, it is important to evaluate the implications that alternative technologies solutions and schemes of a GPP can produce in terms of impacts while performing LCA studies. Therefore, exploiting recent results on GPP simulations studies, a rigorous model of a real plant in Tuscany, Italy, has been developed in UniSim Design® to evaluate the performances in terms of environmental and net energy production of possible alternative scenarios.

Starting from the reference conditions of the dominant water geothermal field of the actual GPP (40 MWe of nominal power), the process simulation models of various possible alternative plant arrangements have been formulated detailing methodologies, assumptions, and criticalities of each one. Based on the indications of the geothermal operator (EGP), the configurations identified for the study, in addition to the basic setup, all share the same gas treatment plant (AMIS®), and they alternate the use of direct-contact and surface condensers as well as wet and dry towers for cooling down the liquid process streams. In addition, also an ORC configuration has been considered. All problems connected with plant engineering and management of re-injection wells were excluded from this study.

Firstly, the model of the actual plant developed from primary data has been reconciled via an optimization procedure with two different datasets, each one collected by EGP under different seasonal conditions. Monitoring four pollutants (Hg, H_2S, NH_3, and SO_2), modeling results have shown an adequate match with the real data with a maximum deviation from the target under 28%, that is, the NH_3 emitted in "*summer*" conditions (33 kg/h calculated against the target, 26.5 kg/h). The largest underestimation (11%) in the emitted quantities is for Hg in "*summer*" conditions, that is 0.8 g/h calculated against 0.9 g/h measured.

Then, a performance comparison of the four alternative configurations simulated has been developed based on quantities emitted and net energy produced. For the sake of brevity, only a comparison based on "*winter*" conditions has been portrayed. The four alternative configurations of the GPP have all been built using the same tuned thermodynamic properties to better represent the behavior of the various pollutants in the various streams and process operations, therefore the results of the simulations are all dependent on the assumptions and methodologies applied. The best results from an environmental point of view are obtained when substituting the wet with the dry tower as a cooling system in which the emissions come from the AMIS®. In particular, a reduction of around 77% in the emitted quantity of H_2S is reached, that is 1.72 kg/h in the best case (dry tower and surface condenser) against 7.67 kg/h measured in the real GPP. Also, the quantities of Hg and NH_3 emitted are much lower than the actual setup and the latter ones can be eliminated with slight acidification of the absorption column in the AMIS®. On the other hand, by substituting the surface condenser with a direct-contact one, emissions of SO_2 are encountered (7.19 kg/h) that can also be easily eliminated by adjusting the alkalinity in the last unit of the AMIS®. Furthermore, greenhouse gas emissions (CO_2 and CH_4) are not affected by the configurations changes since they depend exclusively on the amount of such gases in the well fluid. CO_2 is always the main component in the dry gaseous stream emitted covering 89% of the total flow rate, while CH_4, with almost 280 kg/h, accounts for 2.6%.

A trade-off between environmental performances and net power generation has been evidenced. In fact, the dry towers in both configurations consume more than 1 MWe, specifically, 1.051 MWe for the direct-contact condenser and 1.346 MWe when the surface one is employed. Therefore, the best energy performances come from the configurations with the surface condenser but with the wet tower as a cooling system. The main gain over the basic setup is given by a lower gas flow rate that is entering the AMIS®, causing energy savings on the gas extractor motor. It is also underlined that the analysis portrayed did not include economic aspects such as energy sales prices, network structure, and any benefits that can be applied.

To conclude, this study showed that to properly evaluate GPPs performances, especially when alternative possible configurations are being considered and thus primary data are not an option, rigorous simulation can be a useful tool to extrapolate information and deepen the general notion of a trade-off between environmental and energetic performances.

CRediT authorship contribution statement

Marco Vaccari: Methodology, Software, Formal analysis, Writing. **Gabriele Pannocchia:** Methodology, Formal analysis, Validation. **Leonardo Tognotti:** Methodology, Validation, Supervision. **Marco Paci:** Resources, Data curation, Validation.

Declaration of competing interest

The authors declare that they have no known competing financial interests or personal relationships that could have appeared to influence the work reported in this paper.

Appendix A. Supplementary data

Supplementary material related to this article can be found online at https://doi.org/10.1016/j.renene.2023.03.038.

References

[1] G.W. Huttrer, Geothermal power generation in the world 2015–2020 update report, in: Proceedings World Geothermal Congress, Vol. 2020, 2020, pp. 1–17.

[2] E.T. Sayed, T. Wilberforce, K. Elsaid, M.K.H. Rabaia, M.A. Abdelkareem, K.-J. Chae, A. Olabi, A critical review on environmental impacts of renewable energy systems and mitigation strategies: Wind, hydro, biomass and geothermal, Sci. Total Environ. 766 (2021) 144505.

[3] M. Ozcelik, Environmental and social impacts of the increasing number of geothermal power plants (Büyük Menderes Graben–Turkey), Environ. Sci. Pollut. Res. (2021) 1–13.

[4] C. Tomasini-Montenegro, E. Santoyo-Castelazo, H. Gujba, R. Romero, E. Santoyo, Life cycle assessment of geothermal power generation technologies: An updated review, Appl. Therm. Eng. 114 (2017) 1119–1136.

[5] M.L. Parisi, M. Douziech, L. Tosti, P. Perez-Lopez, B. Mendecka, S. Ulgiati, D. Fiaschi, G. Manfrida, I. Blanc, Definition of LCA guidelines in the geothermal sector to enhance result comparability, Energies 13 (14) (2020) 3534.

[6] Y. Başoğul, Environmental assessment of a binary geothermal sourced power plant accompanied by exergy analysis, Energy Convers. Manage. 195 (2019) 492–501.

[7] Z. Xia, G. Jia, Z. Ma, J. Wang, Y. Zhang, L. Jin, Analysis of economy, thermal efficiency and environmental impact of geothermal heating system based on life cycle assessments, Appl. Energy 303 (2021) 117671.

[8] R. Basosi, R. Bonciani, D. Frosali, G. Manfrida, M.L. Parisi, F. Sansone, Life cycle analysis of a geothermal power plant: Comparison of the environmental performance with other renewable energy systems, Sustainability 12 (7) (2020) 2786.

[9] V. Colucci, G. Manfrida, B. Mendecka, L. Talluri, C. Zuffi, LCA and exergo-environmental evaluation of a combined heat and power double-flash geothermal power plant, Sustainability 13 (4) (2021) 1935.

[10] L. Tosti, N. Ferrara, R. Basosi, M.L. Parisi, Complete data inventory of a geothermal power plant for robust cradle-to-grave life cycle assessment results, Energies 13 (11) (2020) 2839.

[11] M.L. Parisi, N. Ferrara, L. Torsello, R. Basosi, Life cycle assessment of atmospheric emission profiles of the Italian geothermal power plants, J. Clean. Prod. 234 (2019) 881–894.

[12] M. Vaccari, G. Pannocchia, L. Tognotti, M. Paci, R. Bonciani, A rigorous simulation model of geothermal power plants for emission control, Appl. Energy 263 (2020) 114563.

[13] V. Colucci, A. Damone, G. Manfrida, D. Fiaschi, Thermodynamic modelling and simulation of geothermal power plants: case studies and environmental impact, in: EGU General Assembly Conference Abstracts, 2021, pp. EGU21–16182.

[14] J. Granacher, T.-V. Nguyen, R. Castro-Amoedo, F. Maréchal, Overcoming decision paralysis-A digital twin for decision making in energy system design, Appl. Energy 306 (2022) 117954.

[15] N.O. Osinde, J.B. Byiringiro, M.M. Gichane, H. Smajic, Process modelling of geothermal drilling system using digital twin for real-time monitoring and control, Designs 3 (3) (2019) 45.

[16] M.E.H. Assad, Y. Aryanfar, S. Radman, B. Yousef, M. Pakatchian, Energy and exergy analyses of single flash geothermal power plant at optimum separator temperature, Int. J. Low-Carbon Technol. 16 (3) (2021) 873–881.

[17] M. Hijriawan, N. Pambudi, M. Biddinika, D. Wijayanto, I. Kuncoro, B. Rudiyanto, K. Wibowo, Organic rankine cycle (ORC) in geothermal power plants, J. Phys. Conf. Ser. 1402 (4) (2019) 044064.

[18] X. Lu, Y. Zhao, J. Zhu, W. Zhang, Optimization and applicability of compound power cycles for enhanced geothermal systems, Appl. Energy 229 (2018) 128–141.

[19] D. Meng, Q. Liu, Z. Ji, Effects of two-phase expander on the thermoeconomics of organic double-flash cycles for geothermal power generation, Energy 239 (2022) 122346.

[20] N.A. Pambudi, R. Itoi, S. Jalilinasrabady, K. Jaelani, Performance improvement of a single-flash geothermal power plant in Dieng, Indonesia, upon conversion to a double-flash system using thermodynamic analysis, Renew. Energy 80 (2015) 424–431.

[21] B. Rudiyanto, M.A. Bahthiyar, N.A. Pambudi, M. Hijriawan, et al., An update of second law analysis and optimization of a single-flash geothermal power plant in Dieng, Indonesia, Geothermics 96 (2021) 102212.

[22] T. Parikhani, M. Delpisheh, M.A. Haghghi, S.G. Holagh, H. Athari, Performance enhancement and multi-objective optimization of a double-flash binary geothermal power plant, Energy Nexus 2 (2021) 100012.

[23] G. Çetin, A. Keçebaş, Optimization of thermodynamic performance with simulated annealing algorithm: A geothermal power plant, Renew. Energy 172 (2021) 968–982.

[24] C. Yilmaz, I. Koyuncu, Thermoeconomic modeling and artificial neural network optimization of afyon geothermal power plant, Renew. Energy 163 (2021) 1166–1181.

[25] Y. Zhao, B. Du, S. Chen, J. Zhao, Y. Gong, X. Bu, H. Li, L. Wang, Thermo-economic comparison between organic rankine cycle and binary-flashing cycle for geothermal energy, Front. Earth Sci. (2021) 892.

[26] P.H. Niknam, L. Talluri, D. Fiaschi, G. Manfrida, Sensitivity analysis and dynamic modelling of the reinjection process in a binary cycle geothermal power plant of Larderello area, Energy 214 (2021) 118869.

[27] F. Yilmaz, M. Ozturk, R. Selbas, Modeling and design of the new combined double-flash and binary geothermal power plant for multigeneration purposes; thermodynamic analysis, Int. J. Hydrogen Energy 47 (45) (2022) 19381–19396.

[28] J.M. Weinand, R. McKenna, M. Kleinebrahm, K. Mainzer, Assessing the contribution of simultaneous heat and power generation from geothermal plants in off-grid municipalities, Appl. Energy 255 (2019) 113824.

[29] N.A. Pambudi, R. Itoi, S. Jalilinasrabady, M. Gürtürk, Sustainability of geothermal power plant combined with thermodynamic and silica scaling model, Geothermics 71 (2018) 108–117.

[30] G. Manente, A. Bardi, A. Lazzaretto, M. Paci, Low emission flash-binary and two-phase binary geothermal power plants with water absorption and reinjection of non-condensable gases, Geothermics 80 (2019) 155–169.

[31] I. Lee, J.W. Tester, F. You, Systems analysis, design, and optimization of geothermal energy systems for power production and polygeneration: State-of-the-art and future challenges, Renew. Sustain. Energy Rev. 109 (2019) 551–577.

[32] A. Baldacci, M. Mannari, F. Sansone, Greening of geothermal power: an innovative technology for abatement of hydrogen sulphide and mercury emission, in: Proceedings of the World Geothermal Congress, Vol. 2429, Antalya, Turkey, 2005.

[33] P. Kalinkin, O. Kovalenko, V. Khanaev, E. Borisova, Direct oxidation of hydrogen sulfide over vanadium catalysts: I. kinetics of the reaction, Kinetics Catal. 56 (1) (2015) 106–114.

[34] X. Gao, H. Ding, Z. Du, Z. Wu, M. Fang, Z. Luo, K. Cen, Gas–liquid absorption reaction between (NH4) 2SO3 solution and SO2 for ammonia-based wet flue gas desulfurization, Appl. Energy 87 (8) (2010) 2647–2651.

[35] J. Nocedal, S.J. Wright, Numerical Optimization 2nd, Springer, 2006.